ABSTRACT

Title of thesis: MICROWAVE PHOTONS IN HIGH IMPEDANCE TRANSMISSION LINE: DISPERSION, DISORDER AND LOCALIZATION

Nitish Jitendrakumar Mehta, Master of Science, 2017

Thesis directed by: Assistant Professor Vladimir Manucharyan
Department of Physics

In this thesis we will describe the theoretical and experimental studies of a TEM on-chip superconducting transmission line with a wave impedance as high as 20 kΩ, phase and group velocity of waves simultaneously reduced by a factor of 100 in a broad range of frequencies from 0 to about 10 GHz. A conventional microwave coaxial transmission line gets its inductance and capacitance from magnetic and electric fields stored in the space between its inner and outer conductors. This in turn limits its impedance to around 50 Ω and group velocity of waves very close to the speed of light in vacuum. In this work we are able to increase the impedance by over two orders of magnitude and reduce the group and phase velocity of waves by over two orders of magnitude as well, by constructing a coplanar transmission line out of a pair of long Al/AlOx/Al Josephson tunnel junction chains. A Josephson junction gets its inductance not from the magnetic energy but rather from the much larger kinetic energy of tunneling Cooper pairs, which is unrelated to the electromagnetic properties of vacuum. In this work we present a design of such a transmission

line and low-temperature measurement of its dispersion relation. We then study and characterize the disorder present in the circuit parameters of our system and using this, we conclude that for frequencies up to 12 GHz, there is no evidence of Anderson localization of waves, even for chains exceeding 30,000 junctions. Low dissipation and absence of localization make this transmission line ideal for use in various experiments where high impedance can enable strong coupling between light and matter.

MICROWAVE PHOTONS IN HIGH IMPEDANCE TRANSMISSION LINE: DISPERSION, DISORDER AND LOCALIZATION

by

Nitish Jitendrakumar Mehta

Thesis submitted to the Faculty of the Graduate School of the
University of Maryland, College Park in partial fulfillment
of the requirements for the degree of
Master of Science
2017

Advisory Committee:
Professor Thomas Murphy, Chair
Assistant Professor Vladimir Manucharyan, co-Chair/Advisor
Professor Steven Anlage
Professor Christopher Lobb

Acknowledgments

I owe my gratitude to all the people who have made this thesis possible and because of whom my graduate experience has been very fruitful and enjoyable.

First and foremost I'd like to thank my advisor, Professor Vladimir Manucharyan for giving me an invaluable opportunity to work on challenging and extremely interesting projects over the past two years. He has always made himself available for help and advice and there has never been an occasion when I've knocked on his door and he hasn't given me time. It has been a pleasure to work with and learn from such an extraordinary individual.

I would also like to thank my co-advisor, Professor Thomas Murphy. Without his support and valuable guidance throughout my two years, this thesis would have been a distant dream. Thanks are due to Professor Steven Anlage, Professor Christopher Lobb for agreeing to serve on my thesis committee and for sparing their invaluable time reviewing the manuscript.

With a separate paragraph I would like to thank Dr. Roman Kuzmin for teaching me everything from theoretical calculations about Anderson localization to operating the dilution refrigerator and being patient even when I made mistakes repeatedly. Almost all work on this project was done one way or another with either direct or indirect guidance of Roman.

My colleagues at the Superconducting Circuits laboratory have enriched my graduate life in many ways and deserve a special mention. I would like to thank Ray Mencia for fabricating majority of the devices mentioned in this thesis and

helping me understand the fabrication process. Thanks are due to Nicholas grabon for doing the long hours microwave measurements of the device with me. I owe a big thank you to Nathaneal Cottet and Long Nuygen for the numerous hours of debate and discussion, that helped me broaden my vision and helped me see the problem through a different perspective. I would also like to thank Natalia Pankratova, Hanho Lee and Chris for helping me shape my thesis presentation and providing their invaluable input.

I would also like to acknowledge help and support from some of the staff members especially Melanie Prange from the ECE department and Jessica Crosby from the Physics department. I would be lost without their help.

I owe my deepest thanks to my family - my mother and father who have always stood by me and guided me through my career, and have pulled me through against impossible odds at times. Words cannot express the gratitude I owe them.

My housemates at my place of residence have been a crucial factor in my finishing smoothly. I'd like to express my gratitude to Ayan Malik, Proloy Das, Abhishek Chakrobarty for their friendship and support.

It is impossible to remember all, and I apologize to those I've inadvertently left out.

Table of Contents

List of Tables

List of Figures

List of Symbols and Abbreviations

A	area
a	annihilation operator
α	fine structure constant
c	speed of light
C	capacitance per unit length
C_j	junction capacitance
C_{j_n}	capacitance of the nth Josephson junction
C_g	ground capacitance
e	electron charge
E	energy
E_c	charging energy
E_j	Josephson energy
ϵ_0	vacuum permeability
φ	phase across Josephson junction
Φ_0	superconducting flux quantum
h	Plank's constant
$\hbar$	$h/2\pi$
H	Hamiltonian
I	current
I_c	critical current of a Josephson junction
i	summation index; $\sqrt{-1}$
j	summation index
k	wave number
k_n	wave number of mode n
$\mathcal{L}$	Lagrangian
L	inductance per unit length
L_j	Josephson inductance
L_{j_n}	Josephson inductance of nth junction
l_{kin}	kinetic inductance
λ	wavelength
μ_0	permittivity of vacuum
N	number of junctions in an array
π	area of unit circle
Q	charge; quality factor
Q_{int}	internal quality factor
Q_{ext}	external quality factor
R_Q	resistance quantum
ρ	electron density
t	time
τ	reflection coefficient
ω	frequency in radians
ω_0	resonance frequency in radians

ξ	localization length
Y	admittance
Z_0	characteristic impedance of an L-C oscillator
Z_∞	wave impedance of a transmission line

HEMT	High Electron Mobility Transistor
MMA	Methyl Methacrylate
PPMA	Polymethyl Methacrylate
RF	Radio Frequency
SEM	Scanning Electron Microscope
RSCJ	Resistively Shunted Capacitive Junction
VNA	Vector Network Analyzer

Chapter 1: Introduction

One dimensional chains of Josephson junctions have received considerable interest in the last few decades. They were originally introduced as a theoretical model system for the study of the zero-temperature superconductor-insulator transition in superconducting granular films [1] [2]. However, we will study them in the context of making high impedance microwave circuits. Previously, transmission lines have been designed where waves were guided using long strips of aluminium of around 3mm [13] [14]. In this work, we will try to design transmission lines using chains of relatively short, around 0.6μm in length Josephson junctions made into a long chain of 10mm.

In typical radio-frequency electrical circuits, inductances and capacitances come, respectively from magnetic and electric fields stored in the vacuum space between the circuit parts. It turns out that electromagnetic parameters of vacuum, namely the vacuum permeability ϵ_0 and the vacuum permittivity μ_0 restrict the impedance Z_0 of such circuits to low values. As an example we can calculate the impedance of a transmission line formed by two concentric cylindrical parallel wires of radius d_1 and d_2 respectively, short-circuited at one end and left open at the other end, sketched in Figure 1.1. This transmission line can be modeled as a chain

of inductance-capacitance cells where the specific inductance of the wires is calculated to be $L = \mu_0 \ln(d_1/d_2)/2\pi$ and the specific capacitance between the wires is $C = \epsilon_0 2\pi/\ln(d_1/d_2)$. The frequency dependent impedance of the line can then be written using telegraphers equations as [3]

$$Z(\omega) = Z_\infty \frac{e^{i\pi\omega/\omega_0} - 1}{e^{i\pi\omega/\omega_0} + 1} \tag{1.1}$$

$$\omega_0 = \frac{\pi}{2} \frac{1}{\sqrt{LC} \times (\Delta x)} \tag{1.2}$$

$$Z_\infty = \sqrt{\frac{L}{C}} \tag{1.3}$$

The impedance is then given by $Z(\omega \to 0) = i\frac{\pi}{2}\sqrt{\frac{L}{C}}\frac{\omega}{\omega_0}$ at low frequencies, where ω_0 is the resonance frequency of the LC circuit. We can see that the impedance is of the order of the vacuum wave impedance $Z_{vac} = \sqrt{\frac{\mu_0}{\epsilon_0}}$. In this thesis we will show how we can exceed this number using a transmission line made from an array of Josephson junctions.

1.1 Kinetic inductance

From the above discussion it is clear that to build high impedance transmission lines it is necessary to look beyond geometric capacitance and inductance. One way to do it is by harnessing the inductance that originates from the inertia of charge carriers, the so-called kinetic inductance. This phenomenon of kinetic inductance has been used before to design sensitive single photon detectors with applications in radio astronomy [11] [12]. The kinetic inductance per unit length of a wire with cross sectional area A, Cooper pair density ρ and mass of charge carriers m is given

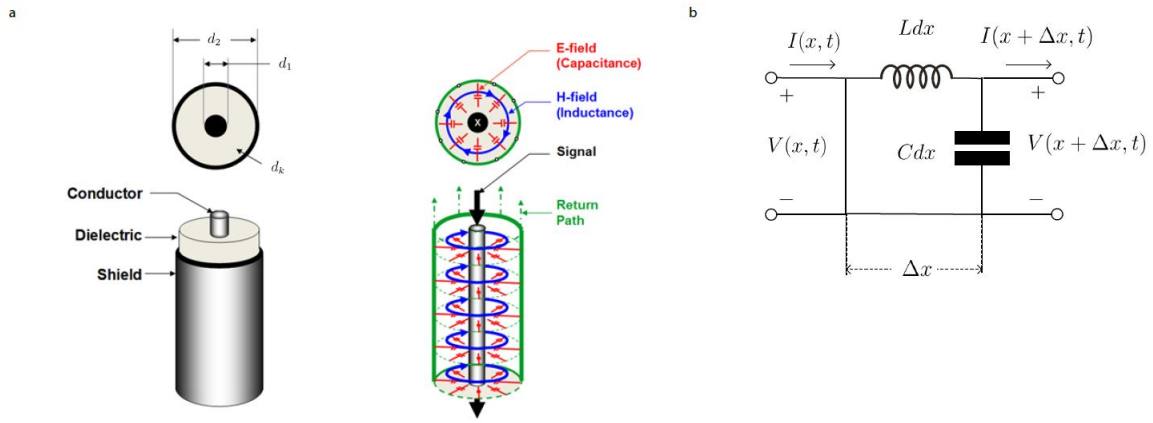

Figure 1.1: (a) A detailed sketch of a coaxial transmission line showing the electrical and magnetic field pattern inside it, (b) Effective lumped element circuit model of a coaxial transmission line.

by [8]

$$l_{kin} = \frac{m}{Ae^2\rho} \tag{1.4}$$

A back of the envelope calculation for a wire 100 nm wide and 10nm thick reveals that the kinetic inductance is still of the order of μ_0, which is no better than the geometric inductance. Equation 1.4 suggests that it is possible to increase kinetic inductance indefinitely by taking Cooper pair density to zero by approaching the superconducting transition temperature , however doing so results in increase of the normal electron density and in turn dissipation.

1.2 High impedance transmission line using Josephson junctions

One way to harness the increase in kinetic inductance of a superconducting wire is by introducing disorder. Disorder decreases the density of Cooper pairs

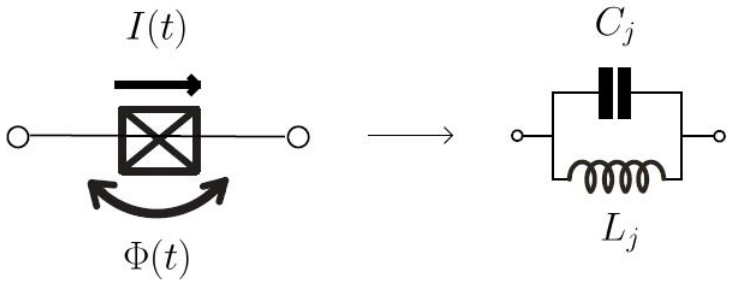

Figure 1.2: Approximation of a Josephson junction to a parallel combination of inductance and capacitance in the linear limit where $\Phi(t) << \Phi_0$ [4]

without the corresponding increase in normal electrons and dissipation. Here the decrease in Cooper pair density is caused by the partial localization of charge carriers. The most clean and controlled way to introduce disorder in a superconductor is to interrupt it with weak links forming Josephson junctions. In Josephson junctions the Cooper pair density is only suppressed inside the weak links. The tunneling of the Cooper pairs across these weak links in a Josephson junction is governed by the properties of the weak link and the difference of the superconducting phase between the two sides of the weak link and is given by the famous Josephson relation which relates the supercurrent flowing through the junction $I(t)$ to the superconducting phase difference across it $\Phi(t)$:

$$I(t) = I_0 \sin\left(\frac{2\pi\Phi(t)}{\Phi_0}\right) \tag{1.5}$$

$$\Phi_0 = \frac{h}{2e} \tag{1.6}$$

Here I_0 is called the critical current of junction and corresponds to the maximum supercurrent that the junction can sustain and Φ_0 is the superconducting flux quan-

tum. Comparing this relation with the linear inductor's current phase relation we can see that if the phase difference between the two terminals of the junction is small we can approximate the Josephson junction as a linear inductor shunted by a capacitance as shown in Figure 1.2. The capacitance comes from the parallel plate capacitor formed by the weak link sandwiched between two superconductors.

$$I(t) = \frac{1}{L}\Phi(t) \tag{1.7}$$

Expanding $\sin\left(\frac{2\pi\Phi(t)}{\Phi_0}\right)$ for small phase difference $\Phi(t) \ll \Phi_0$ and keeping only the leading order term we get

$$I(t) = \frac{2\pi I_0 \Phi(t)}{\Phi_0} \tag{1.8}$$

Where we define the effective inductance of the Josephson junction as:

$$L_j = \frac{\Phi_0}{2\pi I_0} \tag{1.9}$$

We can now get an effective circuit model for the junction as an inductor in parallel with a capacitor and a resistor. This is called the RSCJ model for the the Josephson junction. Although this model has a resistance in parallel with the inductor and a capacitor but in this work we will assume the dissipation in the junction to be negligible, in that case the model reduces to an inductor in parallel with a capacitor.

It is now easy to see that this type of inductance indeed is independent of the vacuum permeability μ_0 and it is possible to beat it by choosing correct junction parameters. For $Al/AlOx/Al$ junctions, the type of junctions which we will be

using for this work, it is easily possible to have inductance per junction to be 1nH, two orders of magnitude higher than the corresponding geometric inductance of aluminium [10].

1.3 Device design

In this section, we describe the design of the devices. The design is very similar to the transmission lines designed by David Haviland to study quantum phase slips [15]. The devices consist of two chains of Josephson junctions running parallel to each other with approximately 10^4 junctions in each chain. The distance between the chains is $10\mu m$. The devices have two capacitor pads one connected to each chain. The pads are $2mm$ away from the device and are used to couple microwaves into the transmission line. As can be seen in the Figure 1.3, the designed transmission line has a mirror or a short on one end of the transmission line and a capacitor which acts like an open circuit at the other end. This geometry and design feature of the transmission line restricts what values the wave number can take and what kind of waves propagate in the transmission line. The voltage waves in the transmission line have to go to a zero on the short side and the current waves have to go to zero on the open side and since both current and voltage are related to each other's first derivative, the voltage wave goes to a maximum when the current wave goes to zero and vise versa. The boundary conditions defined here result in a quantized wave number given by:

$$k_n = \frac{\pi}{2L} + \frac{n\pi}{L} \tag{1.10}$$

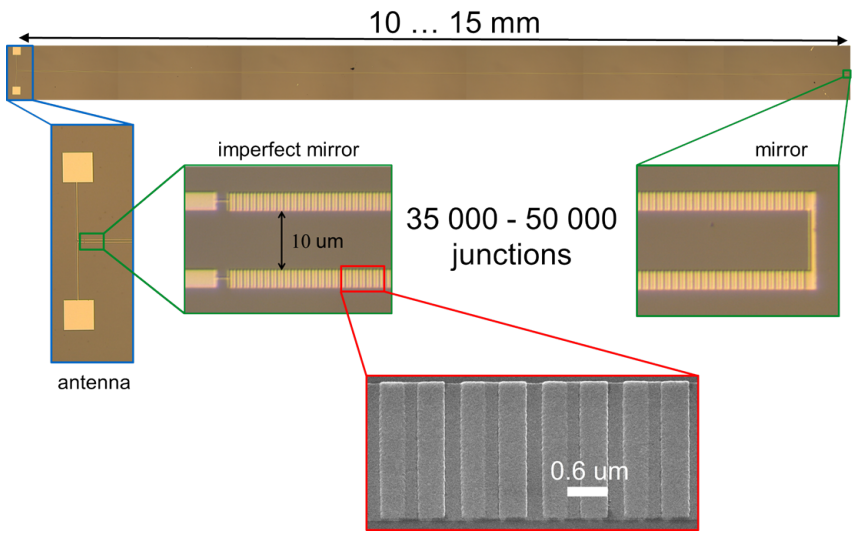

Figure 1.3: An optical image of the transmission line showing its key features. Inset shows the two ends which define the boundary conditions. Another inset shows the SEM image of the junctions that make up the chain.

Here n is the mode number, an integer that starts with 0 and L is the total length of the transmission line. The effective circuit model of the transmission line is shown in Figure 1.4

1.4 Dispersion relation

To obtain the dispersion relation, we start by describing an arbitrary dispersive transmission line. We derive the dispersion for the general case and then apply its result to the case of transmission line made up of Josephson junctions. We can model the transmission line as a frequency dependent impedance and admittance per unit length, defined here as $Z(\omega)$ and $Y(\omega)$ in Figure 1.5 and the length of its unit cell as $a = \Delta x$. We have also defined node voltages and branch currents as

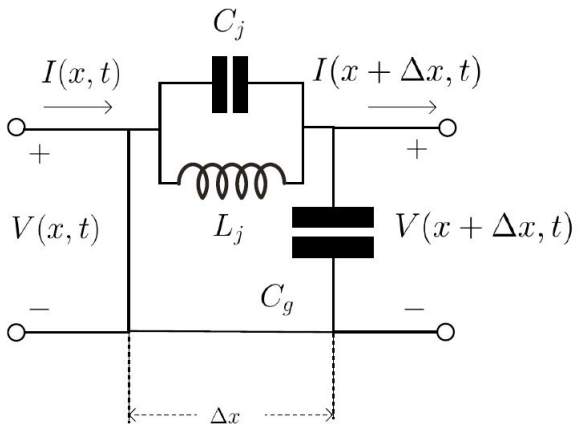

Figure 1.4: Effective circuit model of a transmission line made of Josephson junctions in the linear limit. L_j is the inductance per junction, C_j the capacitance per junction and Δx is the size of the unit cell in the array.

shown Figure 1.5. From the study of telegrapher's equation it is easy to see that such a transmission line admits solutions of node voltages and branch currents that vary sinusoidally both in time and space given by [3]:

$$V_{\uparrow,\downarrow}(x,t) = V_{\uparrow,\downarrow} e^{i(kx-\omega t)} \tag{1.11}$$

$$I_{\uparrow,\downarrow}(x,t) = I_{\uparrow,\downarrow} e^{i(kx-\omega t)} \tag{1.12}$$

In this section we will derive the relation between the wave number k and the frequency ω. It is convenient to work in the frequency domain and hence we define

the Fourier transform in space and time for the currents and voltages as follows:

$$\widetilde{V}_{\uparrow,\downarrow}(x,\omega) = \int_{-\infty}^{\infty} V_{\uparrow,\downarrow}(x,t)e^{-i\omega t}dt \tag{1.13}$$

$$\widetilde{\widetilde{V}}_{\uparrow,\downarrow}(k,\omega) = \int_{-\infty}^{\infty} \widetilde{V}_{\uparrow,\downarrow}(x,\omega)e^{ikx}dx \tag{1.14}$$

$$\widetilde{I}_{\uparrow,\downarrow}(x,\omega) = \int_{-\infty}^{\infty} I_{\uparrow,\downarrow}(x,t)e^{-i\omega t}dt \tag{1.15}$$

$$\widetilde{\widetilde{I}}_{\uparrow,\downarrow}(k,\omega) = \int_{-\infty}^{\infty} \widetilde{I}_{\uparrow,\downarrow}(x,\omega)e^{ikx}dx \tag{1.16}$$

We can now begin to write the Krichoff's loop and junction law to get

$$\widetilde{V}_{\uparrow,\downarrow}(x-\Delta x,\omega) - \widetilde{V}_{\uparrow,\downarrow}(x,\omega) = \widetilde{I}_{\uparrow,\downarrow}(x,\omega)Z \tag{1.17}$$

$$\widetilde{V}_{\downarrow,\uparrow}(x,\omega) - \widetilde{V}_{\uparrow,\downarrow}(x,\omega) = \frac{1}{Y}(\widetilde{I}_{\uparrow,\downarrow}(x+\Delta x,\omega) - \widetilde{I}_{\uparrow,\downarrow}(x,\omega)) \tag{1.18}$$

Dividing equations (1.17) and (1.18) by Δx and taking $\Delta x \to 0$ we get:

$$-\frac{d\widetilde{V}_{\uparrow,\downarrow}(x,\omega)}{dx} = \frac{Z}{a}\widetilde{I}_{\uparrow,\downarrow}(x,\omega) \tag{1.19}$$

$$\widetilde{V}_{\downarrow,\uparrow}(x,\omega) - \widetilde{V}_{\uparrow,\downarrow}(x,\omega) = \frac{a}{Y}\frac{d\widetilde{I}_{\uparrow,\downarrow}(x,\omega)}{dx} \tag{1.20}$$

$$\frac{d\widetilde{I}_{\uparrow}(x,\omega)}{dx} = -\frac{d\widetilde{I}_{\downarrow}(x,\omega)}{dx} \tag{1.21}$$

Since we have assumed harmonic space dependence for both V and I we can replace differentiation with x with multiplying by ik leading to

$$\widetilde{V}_{\uparrow,\downarrow}(x,\omega) = \frac{iZ}{ka}\widetilde{I}_{\uparrow,\downarrow}(x,\omega) \tag{1.22}$$

$$\widetilde{I}_{\uparrow}(x,\omega) = -\widetilde{I}_{\downarrow}(x,\omega) \tag{1.23}$$

Consolidating the results from equations (1.17) to (1.23) we get:

$$-\frac{2iZ}{ka}\widetilde{I}_{\uparrow,\downarrow}(x,\omega) = \frac{aik}{Y}\widetilde{I}_{\uparrow,\downarrow}(x,\omega) \tag{1.24}$$

$$k^2 = -2\frac{Z(\omega)Y(\omega)}{a^2} \tag{1.25}$$

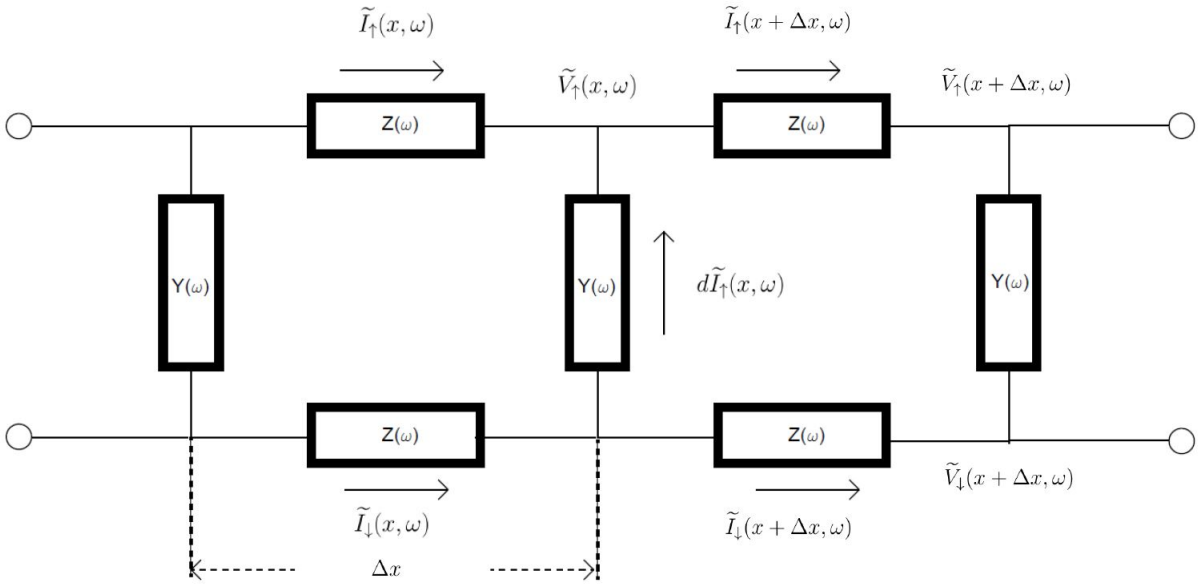

Figure 1.5: Effective circuit model of an arbitrary Transmission line in the frequency domain with the branch currents and node voltages for one section of the line.

Equation (1.25) is the general solution for the dispersion relation for an arbitrary transmission line shown in Figure 1.5.

We can now adapt the expression derived in equation (1.25) for the case of a transmission line made of an array of Josephson junctions. In this case both the Z's are replaced by a Josephson junction and both the Y's are replaced by a capacitor that is formed between the two lines as seen in Figure 1.3. Since we excite the device with low powers of microwaves and we have 35000 junctions in series, it is safe to assume that the phase across each junction is $\ll \Phi_0$. We can then take Z to be the

parallel combination of a capacitor and a linear inductor.

$$\frac{1}{Z(\omega)} = \frac{1}{i\omega L_j} + i\omega C_j \tag{1.26}$$

$$Z(\omega) = \frac{i\omega L_j}{1 - \omega^2 L_j C_j} \tag{1.27}$$

$$Y(\omega) = i\omega C_g \tag{1.28}$$

$$k(\omega) = \sqrt{\frac{2\omega^2 L_j C_g}{(1 - \omega^2 L_j C_j)a^2}} \tag{1.29}$$

We now define two new parameters as:

$$c = \frac{a}{\sqrt{2L_j C_g}} \tag{1.30}$$

$$\omega_p^2 = \frac{1}{L_j C_j} \tag{1.31}$$

$$k(\omega) = \frac{\omega}{c}\sqrt{\frac{1}{1 - (\frac{\omega}{\omega_p})^2}} \tag{1.32}$$

The dispersion defined by equation (1.32) in the limit of $\omega \ll \omega_p$ looks just like a linear dispersion law with effective group and phase velocity of light given by the previously defined parameter c. We can also see that for all frequencies greater than ω_p the wave number becomes imaginary and hence we do not have any propagating wave solutions. The frequency ω_p is called the plasma frequency of the junctions.

Using this we can now plot the final dispersion relation for the transmission line (Figure 1.6) described above and we can also write down the equation for the voltage profile along the transmission line as:

$$V_{k_n}(m) = a_{k_n} \cos k_n(m - 1/2), \quad k_n = \pi/2N, 3\pi/2N \ldots (2N-1)\pi/2N \tag{1.33}$$

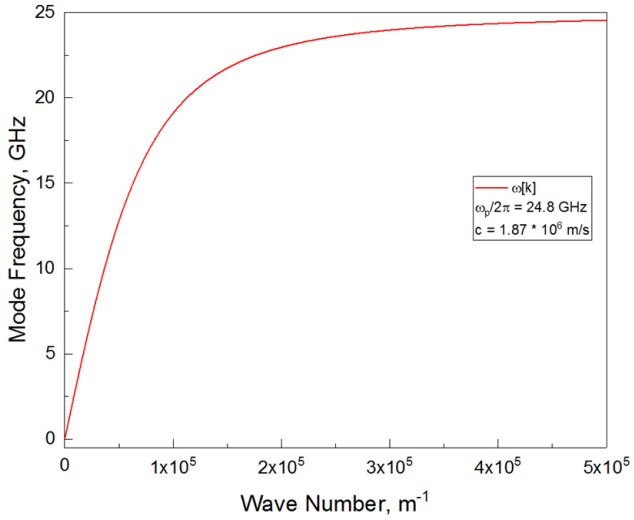

Figure 1.6: A typical dispersion curve plotted for a Josephson junction transmission line where $\omega_p^2 = \frac{1}{L_j C_j}$ and $c = \frac{a}{\sqrt{2L_j C_g}}$.

Where we have defined m as the discrete coordinate along the length of the transmission line.

In summary, we have described a way to design transmission lines with much greater wave impedance than the vacuum impedance using a Josephson junction array, where we harness the kinetic inductance of Cooper pairs. We have then derived the dispersion relation for such a transmission line. Chapter 2 of this thesis will deal with the details of the fabrication and measurement techniques used to characterize the transmission line. Chapter 3 will describe the effect of having disorder in the junction parameters of the transmission line. Finally, Chapter 4 will give a preview of some other exciting experiments that can be done using this transmission line.

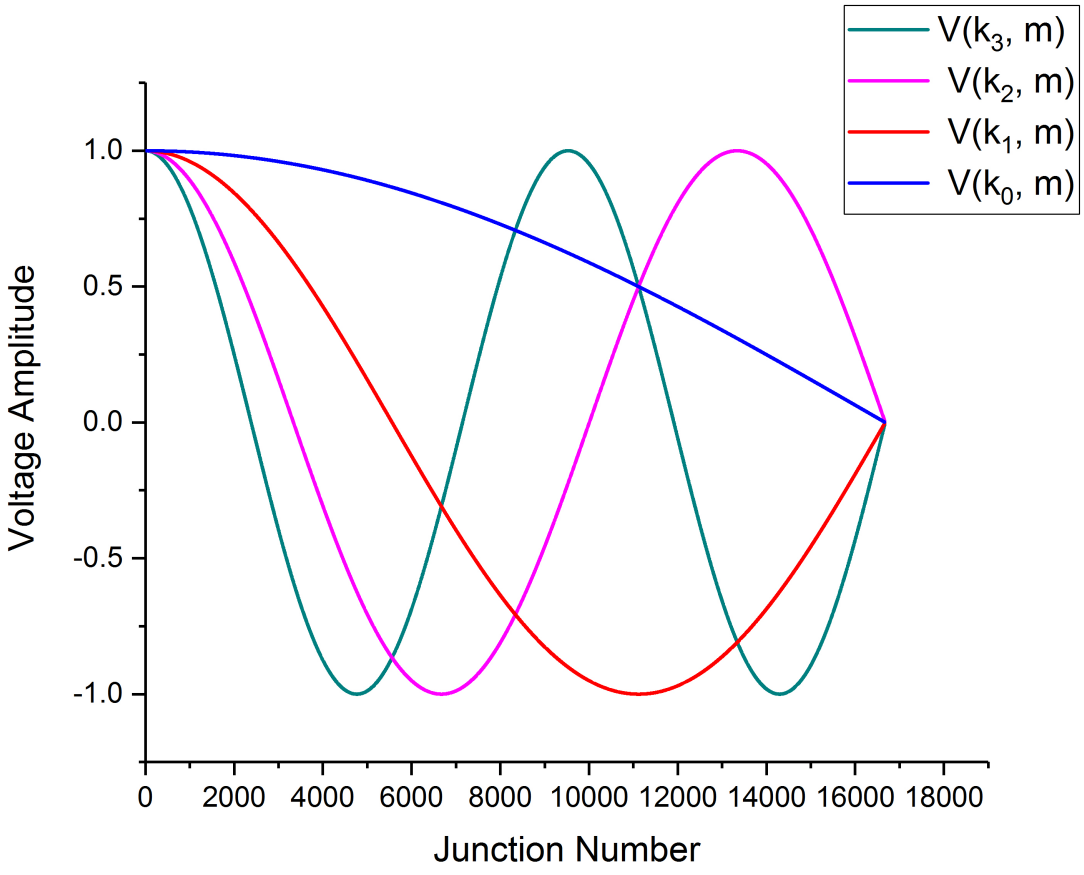

Figure 1.7: Voltage profiles of the first 4 modes in the transmission line given by (1.33).

Chapter 2: Experimental techniques and measurement results

2.1 Fabrication

The sample was fabricated using standard semiconductor processing techniques on a silicon substrate. The silicon substrate is cleaned using solvents and sonication. Next a bilayer of resist is spun on the substrate. The first layer is MMA and the second layer is PMMA. We use a 100 KeV e-beam lithography machine to pattern the mask of the device and develop it in a chilled isopropanol and deionized water solution. The sample is then loaded into a e-beam evaporator and aluminium is deposited using a double angle shadow evaporation technique. The freshly deposited sample is then submerged into hot acetone to dissolve the resist and only leave behind the transmission line.

2.2 Measurement setup

All our experiments on the transmission line are performed in a dilution refrigerator with a base plate temperature of 10 mK. In the setup our goal is to connect our sample to the VNA at room temperature, without letting in the thermal noise and heat from it. We place our sample in a 3-D waveguide which has a single port

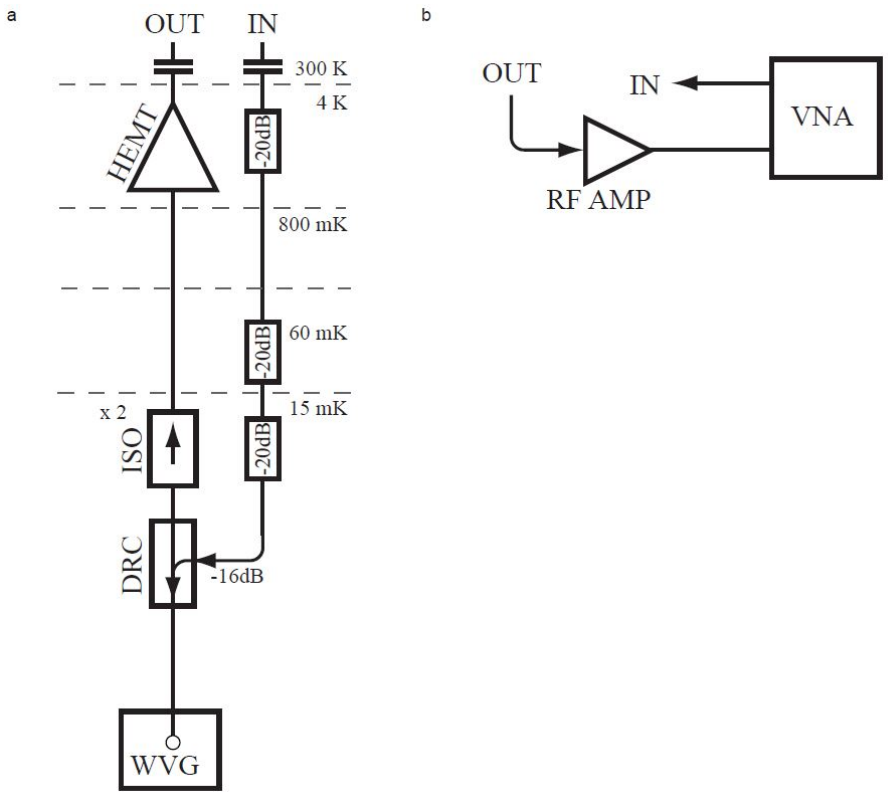

Figure 2.1: (a) The low temperature setup for the reflection measurement of the transmission line. (b) The room temperature setup for the measurement.

to which the coaxial cables are connected. In the input line we place three 20 dB attenuators to remove the thermal noise from the room temperature equipment. We then use a directional coupler to separate the incoming and outgoing signals. On the output line we place two cryogenic isolators to isolate the noise coming in from the HEMT amplifier used at the 4K stage. The outgoing line also has a room temperature RF amplifier to further amplify the signal before it is fed back into the VNA. The schematic of this setup is shown in Figure 2.1.

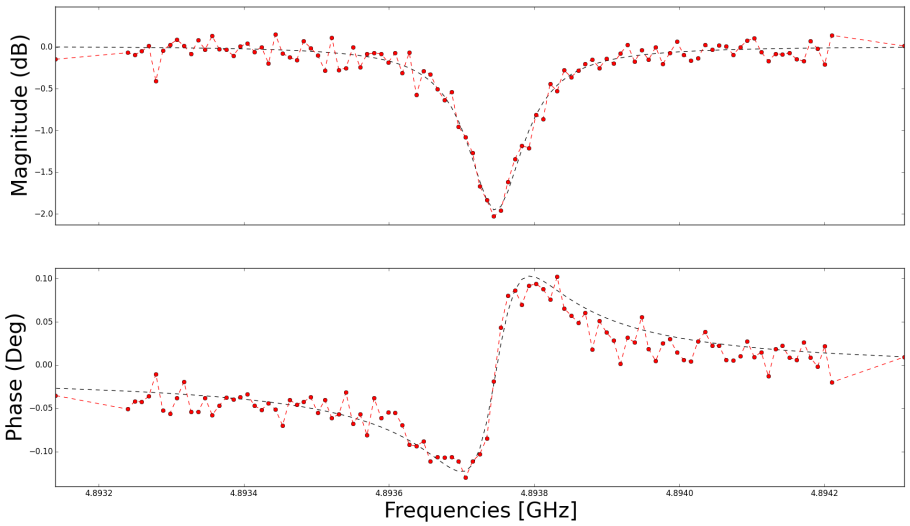

Figure 2.2: Phase and amplitude of the reflection coefficient fitted with equation (2.1) to extract the Q_{int} and Q_{ext}.

2.3 Reflection measurements

We measure the standing wave resonances of the transmission line using a reflection setup as described in the previous section. We can view our transmission line near one of its standing wave resonances as an series LCR circuit capacitively coupled to a 50 Ω transmission line. We can then write the reflection coefficient as [3] [10]:

$$\tau(\omega, \omega_0) = \frac{2i(\frac{\omega-\omega_0}{\omega_0}) - Q_{ext}^{-1} + Q_{int}^{-1}}{2i(\frac{\omega-\omega_0}{\omega_0}) + Q_{ext}^{-1} + Q_{int}^{-1}} \tag{2.1}$$

Where Q_{ext} is the quality factor due to the loss of energy to the coupled coaxial cable and Q_{int} due to the loss inside the sample. For the case of our sample $Q_{int} = R_{int}/Z_0$ and $Q_{ext} = R_{ext}/Z_0$, where Z_0 is the characteristic impedance of our transmission line and R_{int} and R_{ext} are resistances that lump all the internal and external losses of the setup. In summary, using simple reflection measurements and

equation (2.1) it is possible to obtain the frequencies of the standing wave resonances in our transmission line and also fit the measured reflection amplitude to obtain the Q_{ext} and Q_{int} for our device. Figure 2.2 shows the fit for one such standing wave resonance mode of the transmission line.

2.3.1 Two tone spectroscopy

Our measurement setup does not allow us to measure faithfully the reflection coefficients for frequencies below 4 GHz, this is mainly due to the attenuation of the 3-D waveguide into which we place our transmission line as shown in Figure 2.3. To overcome this limitation we can use a trick called two tone measurement to measure the positions of resonances in our transmission line below 4 GHz. We take advantage of the lowest order non-linearity in our system, which couples every mode in the transmission line with every other mode, as can be seen from the Hamiltonian of the system derived in Appendix A. We can easily see that the frequency of each mode depends on the population of every other mode (A.17). So, we can measure the position of a low frequency resonance by monitoring reflection amplitude of a known resonance in the pass band of the 3-D waveguide. We first choose an appropriate frequency as a readout frequency and observe the reflection amplitude at this frequency while simultaneously driving a second tone to search for modes in the $0 - 4$GHz range, as the second driving tone passes through a resonance the reflection amplitude will change as shown in the Figure 2.4, giving us the position of the standing wave resonance.

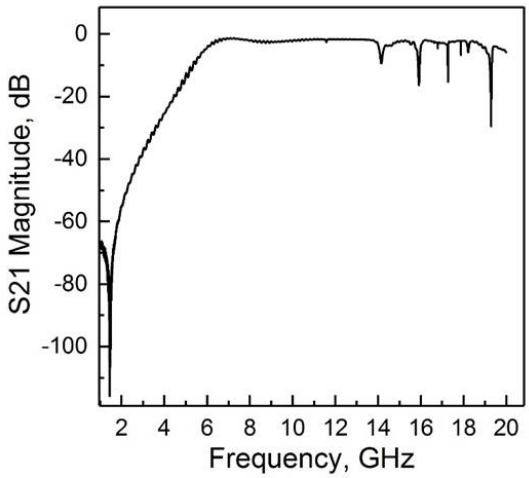

Figure 2.3: The plot shows the transmission spectrum of the 3-D waveguide into which the transmission line is placed.

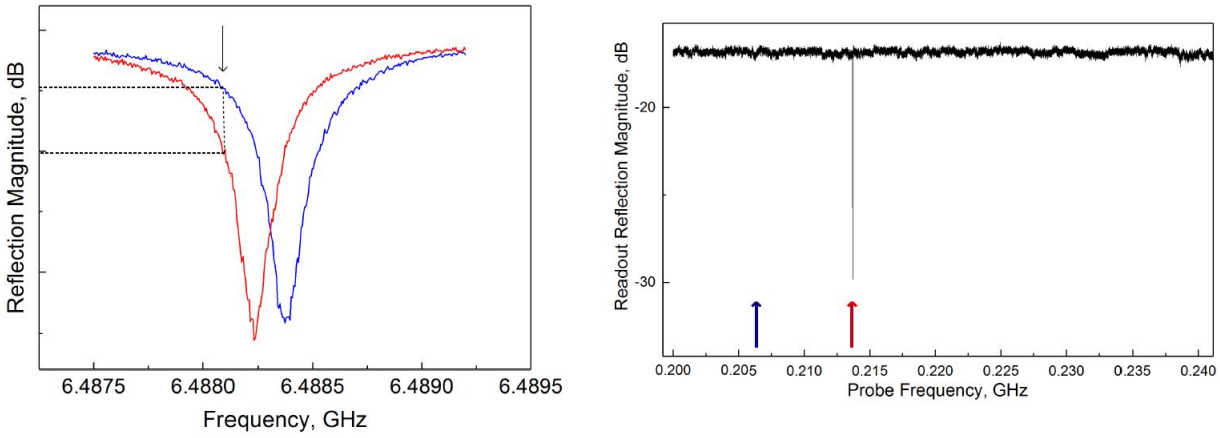

Figure 2.4: Change in the reflection amplitude profile when a second tone is driven at two different frequencies. (a) Shows the shift in the resonance frequency and the black arrow shows the selection of readout frequency. (b) The reflection amplitude at the readout frequency while sweeping the second tone.

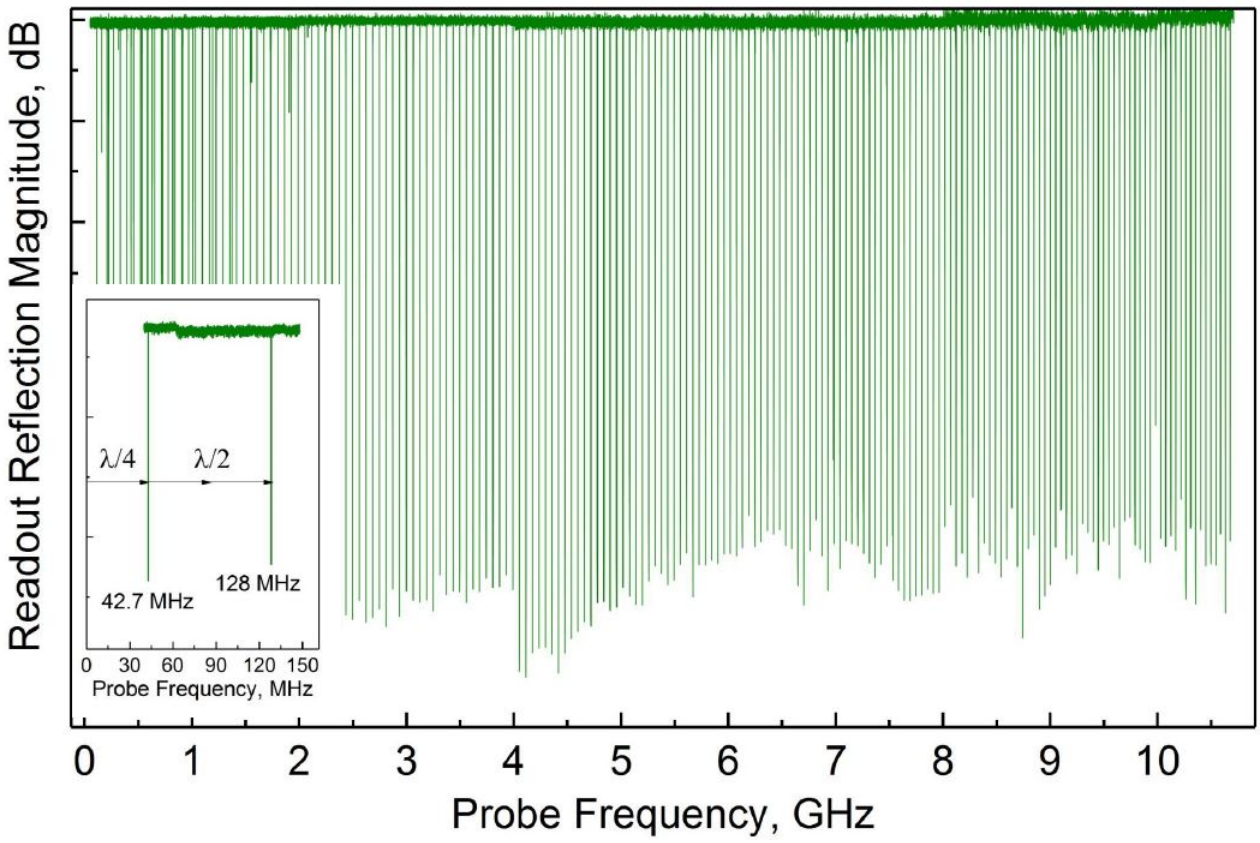

Figure 2.5: The comb of standing wave resonances measured for the transmission line from 0 to 10 GHz. The inset shows the first λ /4 mode and the spacing between the modes given by $\lambda/2$.

2.4 Measurement results

Using the normal reflection measurements and two tone measurements it is possible to find out positions of all standing wave resonances in the transmission line up to 12 GHz. Figure 2.5 shows the full spectrum of the transmission line modes in a broadband range from 0 to 10 GHz. Equipped with this data, it is now possible to fit the dispersion relation for the transmission line derived in chapter 1 in equation (1.32). In Figure 2.7 and Figure 2.6 we show several such fits and table

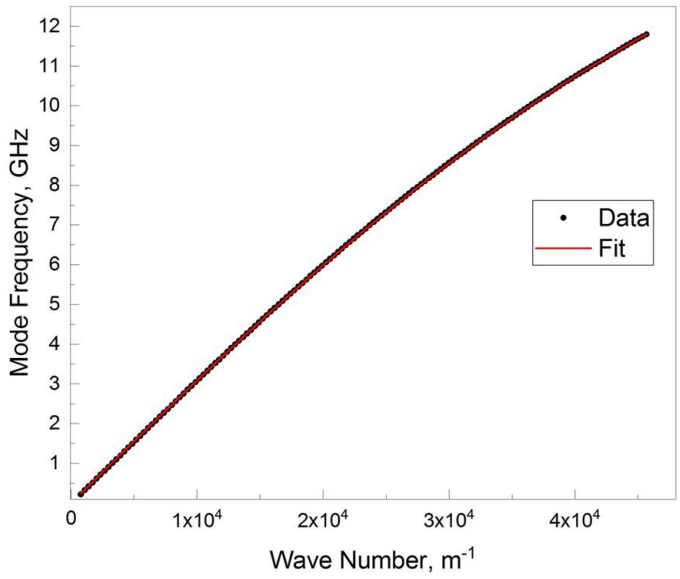

Figure 2.6: Fit of the dispersion curve to the equation (1.32) to extract the group velocity of light in the transmission line and the characteristic impedance of the transmission line.

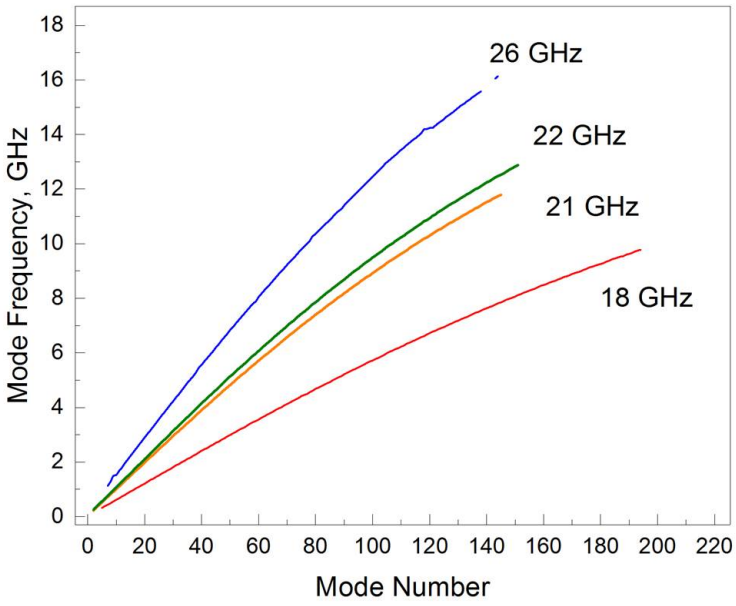

Figure 2.7: Measured dispersion curve for several devices with plasma frequencies, tabulated in Table 2.1.

2.1 shows the extracted parameters from the fit.

Table 2.1: Parameters of transmission lines measured.

Plasma frequency (GHz)	Group Velocity of Light (m/s)	Characteristic Impedance (kΩ)
21	2.1 $\times 10^6$	6.8
18	1.8 $\times 10^6$	7.9
26	2.8 $\times 10^6$	8.1

2.4.1 Beyond linear measurements

As mentioned in Appendix A, the Josephson junction is actually a non-linear inductor. When we consider the lowest order non-linear term in the expansion of equation (1.6) we find that the Hamiltonian of the system has a fourth order quartic non-linearity, as mentioned in equation (A.16). To characterize the non-linear term we measure reflection amplitude for standing wave resonance modes of the transmission line for different drive powers ranging from -50dBm to -15dBm. The resulting curves fit perfectly to the Duffing oscillator model as shown in Figure 2.8 [16]. This measurement gives us a very good understanding of the non-linearity present in our system and the range of powers where the linear approximation of the Josephson junction is valid for our transmission line.

In the measurements made on the transmission line, we also see possible evidence of quantum effects. The internal quality factors of resonances were measured for transmission lines made with different junction parameters, in particular the E_j/E_c was changed by changing the area of the junctions. E_j and E_c of a junction

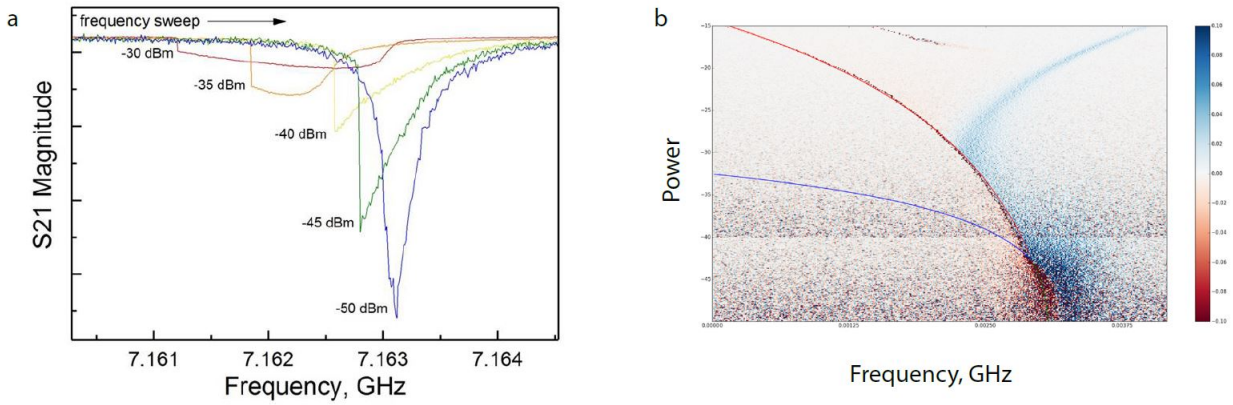

Figure 2.8: (a) Plot showing the reflection amplitude measurement for a standing wave mode of the transmission line for different applied powers of the driving tone. (b) Fit of the data to the Duffing model.

are the Josephson energy and the charging energy of the junctions as defined in Appendix A. The results plotted in Figure 2.9 show a sharp drop in the internal quality factor below a threshold value of $E_j/E_c = 15$. This could be explained by the increase in the probability of quantum phase slips across the junctions, which is proportional to $e^{-\sqrt{8E_j/E_c}}$ [15]. When the phase slips across the junctions are incoherent they cause dissipation and the dissipation from these effects becomes more important as E_j/E_c is reduced and the correlation length becomes comparable to the size of the chain or the wavelength of photons inside the transmission line. The correlation length is defined as the length of the chain where at least one phase slip occurs.

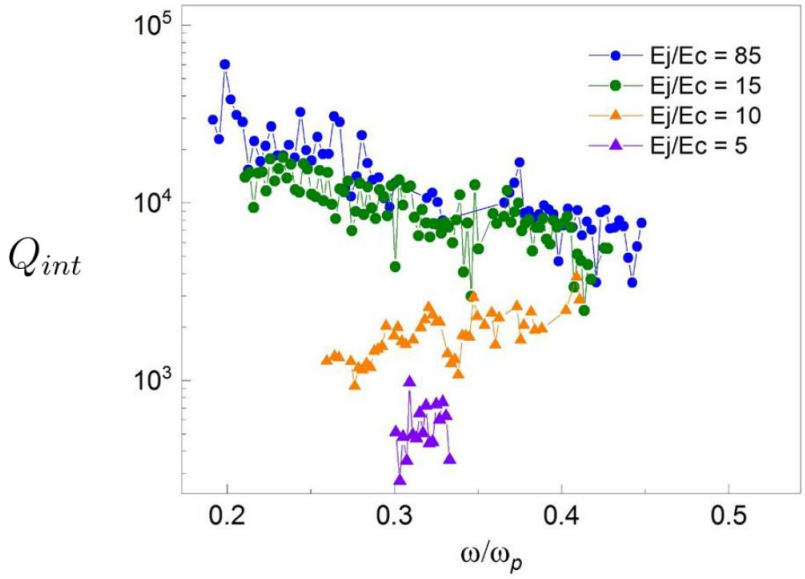

Figure 2.9: The plot shows internal quality factor of resonances for transmission lines with different E_j/E_c plotted against normalized frequency. It is easy to notice the sharp drop in quality factors below a threshold value of $E_j/E_c = 15$.

Chapter 3: Disorder in transmission line parameters

3.1 Overview

Our transmission line consists of an array of around 10^4 nominally identical Josephson junctions made using e-beam lithography. Like any other manufacturing process this too has its uncertainties and imperfections which can result in a circuit different than the one originally designed. Fabrication of the device is sensitive to a large number of parameters which in general are very hard to control. This causes non-uniformities in the parameters of individual junctions as shown in Figure 3.2. These non-uniformities do not cause a big change in the overall properties of the transmission line like the characteristic impedance, the group velocity of light or the plasma frequency of the device because the effect of these small fluctuations is averaged out over 10^4 junctions. However, the measurement of mode frequencies is sensitive to this disorder and it is possible to characterize the disorder in our device by comparing the measured positions of the standing wave resonances to the fit of the dispersion curve. Figure 3.1 shows the comparison between the measured mode frequencies with the fit of the dispersion curve. In the next section we will describe in detail how it is possible to use this data to recover the disorder in the transmission line.

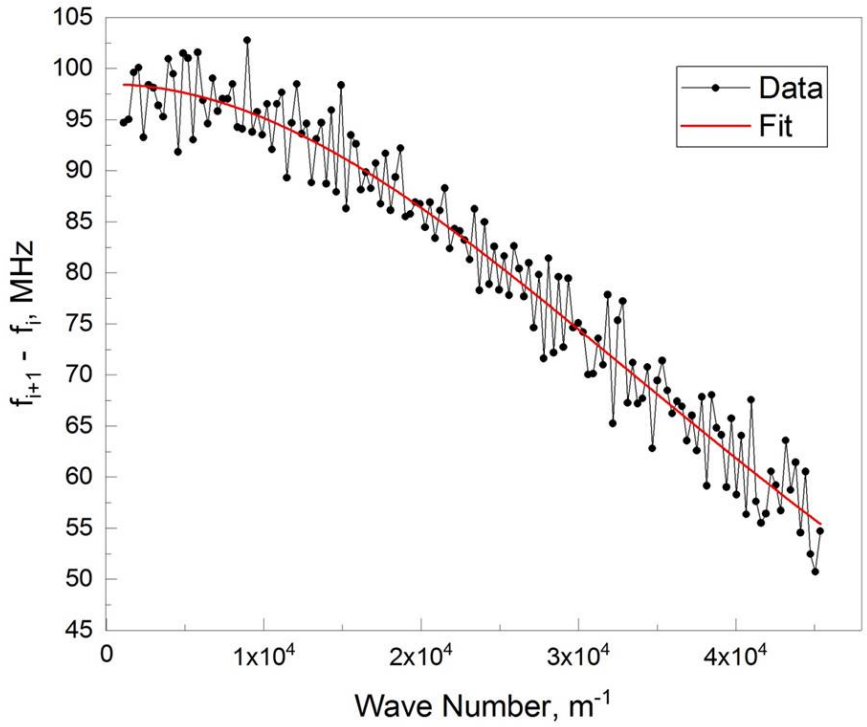

Figure 3.1: Plot of mode spacing with mode number showing the difference of the measured frequencies to the fit.

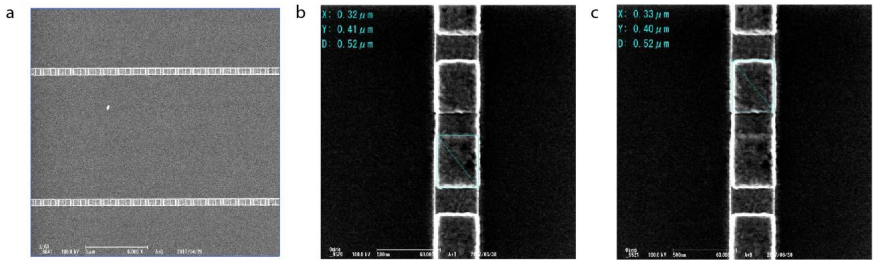

Figure 3.2: Pictures showing the disorder in area of the junctions. Pictures in (b) and (c) show areas can differ up to 10 percent within the same chain.

3.2 Disorder model

The disorder in our junction parameters can result from a number of reasons ranging from lithography errors to difference in the growth of the oxide. In this work we assume the disorder to result solely from the uncorrelated variation of area from junction to junction. This model leads to a disorder given by:

$$\widetilde{L}_{jn} = L_j/(1+\zeta_n) \tag{3.1}$$

$$\widetilde{C}_{jn} = C_j(1+\zeta_n) \tag{3.2}$$

Here L_{j_n} and C_{j_n} are the inductance and capacitance of the nth junction and ζ_n is the disorder parameter for the nth junction. We have assumed $\zeta_n \ll 1$. Since the inductance of the junction scales as the inverse of the junction area and the capacitance of the junction scales as the area of the junction therefore, in this model the plasma frequency does not change from junction to junction. We can now relate the variation of the mode frequencies to the disorder using the result [9]:

$$\delta\omega_\alpha = \Big(\frac{1}{\omega_\alpha L_j} - \omega_\alpha C_j\Big) \sum_{n=0}^{N-1} \zeta_n (V_{\alpha,n+1} - V_{\alpha,n})^2 \tag{3.3}$$

This relation uses the voltage profile for a mode of the transmission line with wave number k_α and relates it to the deviation in the frequency of the mode from the average fit value $\delta\omega_\alpha$. Substituting the value for the voltage profiles from equation (1.33) we can get the relation as:

$$\delta\omega_\alpha = 2\Big(\frac{1}{\omega_\alpha L_j} - \omega_\alpha C_j\Big) \cos^2(k_\alpha) \sum_{n=0}^{N-1} \zeta_n \big(\cos(2k_\alpha n) - 1\big) \tag{3.4}$$

3.3 Extracting disorder

Now that we have the relation between the frequency shifts and the disorder in junction sizes we can start to use this relation to extract disorder for some of the devices that we have measured. The first issue that we run into here is that we need to solve the equation (3.4) which has N variables (ζ_n) but we can only measure the frequency of around 200 modes which is $\ll N$, so we only have 200 equations to solve for around 10000 variables. At first glance this might look like an unsolvable problem but if we look closely at the equation (3.4), we observe that the frequency shifts are just the Fourier transform of the spatial disorder, so to get the spatial disorder all we need to do is apply an inverse Fourier transform to the frequency shifts measured. The fact that we do not have all the frequency components will limit in the accuracy of the disorder profile retrieved but does not preclude us from solving equation (3.4). We can also notice that since the transmission line modes obey the open-short boundary condition, we can only reconstruct disorder in the transmission line that is odd, if we also had the transmission with the same parameters but an open-open boundary condition, we would be able to reconstruct the even part of the disorder profile.

Below we show the disorder reconstructed for two different transmission lines. First is a transmission line which has a periodic fluctuation in inductance every 0.5mm and the second which doesn't have any such fluctuation. We can see in Figure 3.3 that it is possible to reproduce faithfully the periodic fluctuations in inductance using just the frequency measurements as describe above. Using these reconstructed

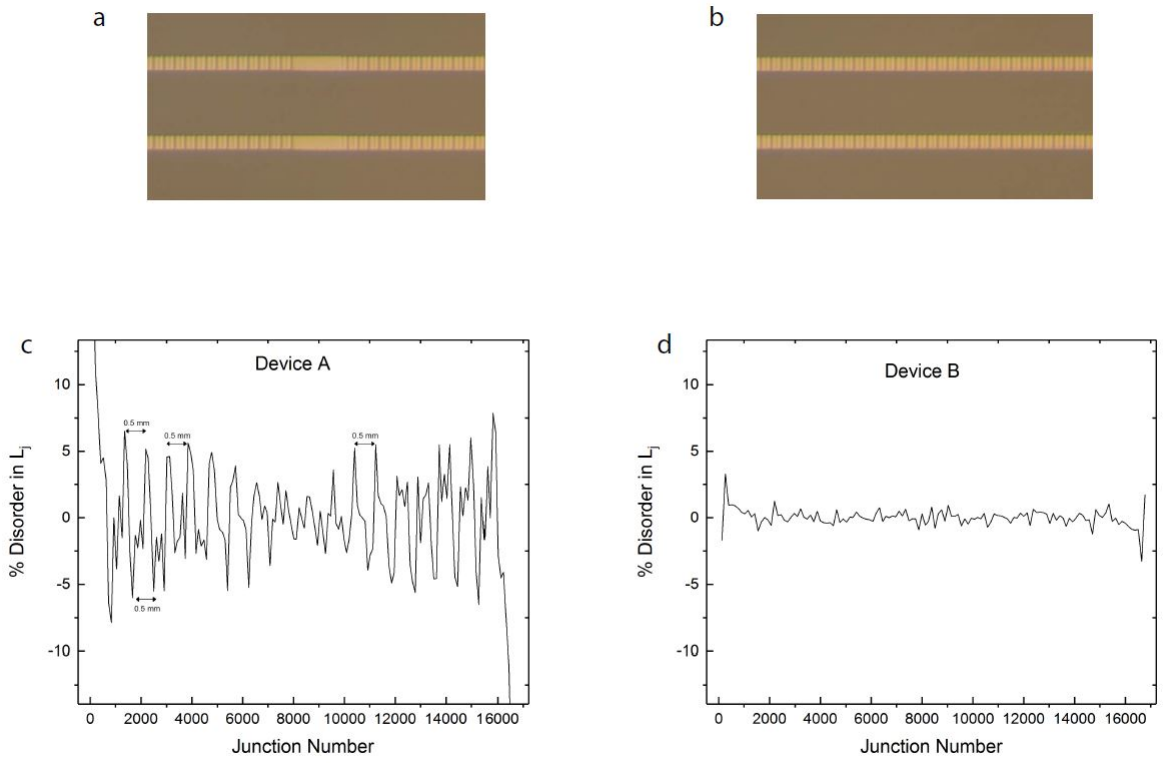

Figure 3.3: (a) and (b) show optical images of two transmission line devices, one with a periodic disorder every $0.5mm$ in the chain and other with no such visible disorder. Plots (c) and (d) show the disorder extracted by measuring the frequencies of the two devices, plot (c) accurately reproduces the periodic disorder with the correct spacing.

disorder profiles, we can also place an upper limit on the actual disorder we have in our junction parameters to 10%. We will use these measurements to investigate if we expect to have localized waves in our transmission lines.

3.4 Anderson localization

Anderson localization is a general wave phenomenon characterized by the absence of wave propagation or diffusion in a disordered medium. In general, the effects of localization and dissipation are hard to distinguish because both result

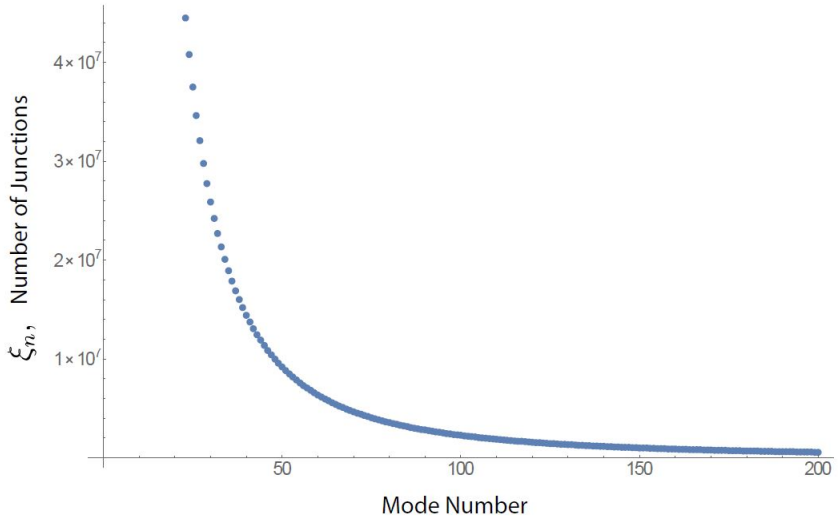

Figure 3.4: Plot of localization length in the transmission line with 10 per cent Gaussian disorder in area. It is easy to see that the localization length is two orders of magnitude greater than the number of junctions in the transmission line.

in exponentially suppressed waves in the medium. In our case, since we deal with superconducting transmission lines, we can safely ignore the effects of dissipation and try to investigate the effects of localization. We can use the theoretical result to get an estimate of the localization length in our transmission line given the upper bound of 10% Gaussian disorder from the previous section [9] as:

$$\frac{1}{\xi_n} = \frac{\sigma^2}{2} \tan^2 \frac{k_n}{2} \tag{3.5}$$

Where ξ_n is the localization length for mode with wave number k_n measured in number of junctions and σ is the standard deviation of the disorder. As can be seen from the Figure 3.4, the localization length predicted for our disorder and junction parameters turns out to be at least two orders of magnitude higher than

the total length of the transmission line measured in number of junctions. We can also argue the absence of localization by looking at the plot of the fitted external quality factors of mode resonances with the mode frequency in Figure 3.5. Since the external quality factors remain roughly constant over the frequency space where our 3-D waveguide has a flat transmission coefficient (6GHz to 10GHz), we safely assume the absence of localization. The presence of localization would make it very hard to couple to localized modes in the given reflection setup and would result in a sudden increase of Q_{ext}, which we do not observe.

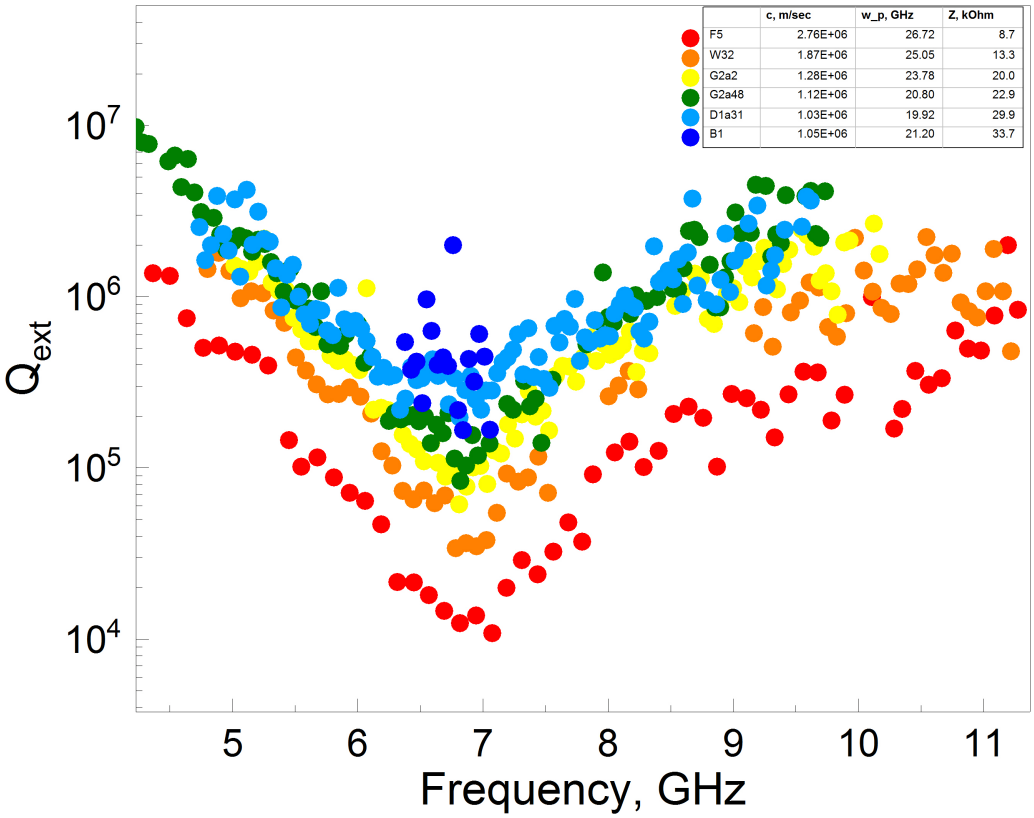

Figure 3.5: This figure shows the variation of Q_{ext} with mode frequency for a collection of devices. The main point to note here is that the Q_{ext} for modes in the rage of 6 to 10 GHz does not change drastically as would be expected if the modes were localized.

Chapter 4: Conclusions and future work

In this work we presented theoretical and experimental studies of a high impedance transmission line with an impedance as high as 20 kΩ and group velocity of light reduced by a factor of over 150. We also characterized the disorder in the junction parameters and showed that given the positions of the standing wave resonances in a device it is possible to reconstruct variation in the circuit parameters. These measurements can be very sensitive to disorder and can find variations in junction parameters not possible to detect by SEM images. We also gave evidence of absence of localized modes in our transmission line using the disorder measurements.

Moving forward these devices can be used for quantum simulations with environments where electromagnetic radiation couples to matter much more strongly when compared to free space. The coupling of electromagnetic radiation to matter is governed by a dimensionless number α called the fine structure constant given by:

$$\alpha = \frac{1}{4\pi\epsilon_0}\frac{e^2}{\hbar c} \tag{4.1}$$

This number for the case of free space turns out to be $\alpha_{vac} \approx \frac{1}{137}$, and puts a limit on how strongly electromagnetic radiation can couple to matter. It is also possible to write this number in terms of the vacuum impedance and the superconducting

resistance quantum given by:

$$R_Q = \frac{h}{4e^2} \approx 6.5k\Omega \tag{4.2}$$

$$Z_0 = \sqrt{\frac{\mu_0}{\epsilon_0}} \approx 377\Omega \tag{4.3}$$

$$\alpha = \frac{Z_0}{8R_Q} \tag{4.4}$$

The equation 4.4 proves that in an environment where the characteristic impedance is of the order of resistance quantum, we can have an effective fine structure constant to be of the order of unity. This condition is fulfilled for the case of the metamaterial that is our transmission line. The next step is then to try to couple artificial atoms to the microwave photons in the transmission line and explore quantum electrodynamics in the regime with $\alpha \approx 1$.

Appendix A: Circuit Hamiltonian

In this Appendix we will calculate the circuit Hamiltonian from the circuit model [7] shown in Figure A.1. The most important result here is coupling between different modes that arises by taking into consideration the first non-linear term from the cosine potential of the Josephson junctions. This coupling is important because it is exploited in measuring the low frequency modes of the transmission line using the two tone spectroscopy method.

The Lagrangian of the system can be written in terms of the node fluxes as:

$$\mathcal{L} = (2e)^2 \sum_{n=1}^{N-1} \frac{\dot{\Phi}_n^2}{2E_g} + \frac{C_{in}\dot{\Phi}_0^2}{2} + \frac{C_{out}\dot{\Phi}_N^2}{2} + (2e)^2 \sum_{n=0}^{N-1} \frac{(\dot{\Phi}_{n+1} - \dot{\Phi}_n)^2}{2E_c} - E_j \sum_{n=0}^{N-1} \cos(\Phi_{n+1} - \Phi_n) \tag{A.1}$$

where E_j is the Josephson energy of the junction and we have defined the charging energies for the ground and Josephson capacitances as follows:

$$E_g = \frac{(2e)^2}{C_g} \tag{A.2}$$

$$E_c = \frac{(2e)^2}{C_j} \tag{A.3}$$

We can now write the Lagrangian of the system in the linear regime which is just

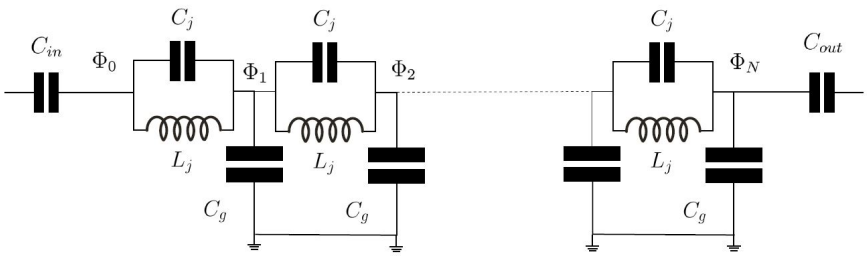

Figure A.1: The Figure shows the circuit diagram of a transmission line made of a ladder of N Josephson junctions here approximated by a linear inductor of inductance L_j shunted with a capacitance C_j and ground capacitance C_g. In our system we have a finite input capacitance that arises from our capacitor pads in the device but a zero output capacitance because of a short at one end of the device.

the difference of the kinetic energy and the potential energy as:

$$\mathcal{L} = \sum_{n=1}^{N-1} \frac{\dot{\Phi}_n^2 C_g}{2} + \frac{C_{in}\dot{\Phi}_0^2}{2} + \frac{C_{out}\dot{\Phi}_N^2}{2} + \sum_{n=0}^{N-1} \frac{(\dot{\Phi}_{n+1} - \dot{\Phi}_n)^2 C_j}{2} - \sum_{n=0}^{N-1} \frac{(\Phi_{n+1} - \Phi_n)^2}{2L_j} \tag{A.4}$$

This can be easily written in a compact form using matrices for capacitances and inductances as follows:

$$\hat{C} = \begin{bmatrix} C_j + C_{in} & -C_j & 0 & . & . & . \\ -C_j & C_g + 2C_j & -C_j & . & . & . \\ 0 & -C_j & C_g + 2C_j & -C_j & . & . \\ . & \ddots & \ddots & \ddots & \ddots & \end{bmatrix} \tag{A.5}$$

$$\hat{L}^{-1} = \begin{bmatrix} \frac{1}{L_j} & -\frac{1}{L_j} & 0 & . & . & . \\ -\frac{1}{L_j} & \frac{2}{L_j} & -\frac{1}{L_j} & . & . & . \\ 0 & -\frac{1}{L_j} & \frac{2}{L_j} & -\frac{1}{L_j} & . & . \\ . & \ddots & \ddots & \ddots & \ddots & \end{bmatrix} \tag{A.6}$$

$$\mathcal{L} = \frac{1}{2}\hat{\dot{\Phi}}^T \hat{C} \hat{\dot{\Phi}} - \frac{1}{2}\hat{\Phi}^T L^{-1} \hat{\Phi} \tag{A.7}$$

We then do the usual Legendre transform to get the Hamiltonian:

$$\hat{Q} = \hat{C}\hat{\dot{\Phi}} \tag{A.8}$$

$$H = \frac{1}{2}\hat{Q}^T \hat{C}^{-1} \hat{Q} + \frac{1}{2}\hat{\Phi}^T \hat{L}^{-1} \hat{\Phi} \tag{A.9}$$

We can now convert this Hamiltonian into an eigenvalue problem where the eigenvalues give us the frequencies of the mode.

$$\hat{\phi} = \hat{C}^{-1/2}\hat{\Phi} \tag{A.10}$$

$$E = \frac{1}{2}\hat{\dot{\phi}}^2 + \frac{1}{2}\hat{\phi}^T \hat{C}^{-1/2} \hat{L}^{-1} \hat{C}^{-1/2} \hat{\phi} \tag{A.11}$$

Assuming harmonic dependence in time of the flux vector we get:

$$\hat{\psi}(t) = \sum_j \hat{\psi}_j (\varphi_j^* e^{-i\omega_j t} + \varphi_j e^{i\omega_j t}) \tag{A.12}$$

$$\hat{C}^{-1/2} \hat{L}^{-1} \hat{C}^{-1/2} \hat{\psi}_j = \omega_j^2 \hat{\psi}_j \tag{A.13}$$

Quantifying the variable φ as in the case of a harmonic oscillator, we find the quantum Hamiltonian. The Hamiltonian reduces to a collection of uncoupled quantum harmonic oscillators.

$$\hat{\varphi} = \sqrt{\frac{\hbar}{2\omega_j}} \hat{a}_j \tag{A.14}$$

$$\hat{H} = \sum_{j=1}^{N} \hbar\omega_j \left(\hat{a}_j^\dagger \hat{a}_j + \frac{1}{2} \right) \tag{A.15}$$

We can now go ahead and include the lowest nonlinear contribution to the Hamiltonian, which comes from the cosine term of the Josephson potential. The leading

order term in the potential is given by:

$$H' = -\frac{E_j}{24\Phi_0^4}\sum_{n=1}^{N-1}(\Phi_{n+1} - \Phi_n)^4 \tag{A.16}$$

Expanding expression (A.16) by substituting the value from equation (A.11) we find that the Hamiltonian contains all possible combinations of fourth order terms in the annihilation and creation operators. The terms we are interested in are of the form $\hat{a}_j^\dagger \hat{a}_j \hat{a}_k^\dagger \hat{a}_k$ with $j \neq k$ and of the form $\hat{a}_j^\dagger \hat{a}_j \hat{a}_j^\dagger \hat{a}_j$. These terms, when added to the linear Hamiltonian, couple all the modes with each other where the frequency of each oscillator is renormalized depending on the the population in every other mode including itself. The nonlinear Hamiltonian including these terms has the form:

$$H_{nl} = \frac{16\pi^4 E_j}{24\Phi_0^4}\Big[\sum_{j\neq k}\frac{\kappa_{jjkk}}{\omega_j\omega_k}(\hat{a_j} + \hat{a_j}^\dagger)^2(\hat{a_k} + \hat{a_k}^\dagger)^2 + \sum_j \frac{\kappa_{jjjj}}{\omega_j^2}(\hat{a_j} + \hat{a_j}^\dagger)^4\Big] \tag{A.17}$$

The terms in the non-linear Hamiltonian of the form $\hat{a}_j^\dagger \hat{a}_j \hat{a}_j^\dagger \hat{a}_j$ renormalizes the frequency of a mode depending on the population of the mode itself. This gives rise to the Duffing type quartic non-linearity in our system.

Bibliography

[1] K. B. Efetov, Sov. Phys. JETP 51, 1015 (1981).

[2] R. M. Bradley and S. Doniach Phys. Rev. B 30, 1138 (1984).

[3] David M. Pozar *Microwave Engineering, fourth Edition* (2005).

[4] B.D. Josephson *The discovery of tunnelling supercurrents* Rev. Mod. Phys. 46, 251254 (1974)

[5] T. Weil PhD Thesis, Universite Joseph Fourier (2014).

[6] F. Lecocq, I. M. Pop, Z. Peng, I. Matei, T. Crozes, T. Fournier, C. Naud, W. Guichard, and O. Buisson , Nanotechnology 22, 315302 (2011).

[7] T. Weil et. al *Kerr Coefficients of Plasma Resonances in Josephson Junction chains* Phys. Rev. B 92, 104508 (2015).

[8] A. J. Annunziata, et al., Nanotechnology 21, 445202 (2010)

[9] D. M. Basko et al. , Physical Review B 88, 094507 (2013)

[10] V. E. Manucharyan, PhD Thesis, Yale University (2012)

[11] A. J. Annunziata, et al., Applied Superconductivity, IEEE Transactions on Applied Superconductivity on 19, 327 (2009).

[12] P. K. Day, H. G. LeDuc et al. Nature 425, 817 (2013)

[13] O. Buisson, P. Xavier and J. Richard, Physical Review Letters 23, 73 (1994)

[14] O. Buisson and J. Richard, IEEE Transactions on Applied Superconductivity on 5, 2 (1995)

[15] Adem Ergul, Jack Lidmar et al., New Journal of Physics, 15, 095014 (2013)

[16] V. E. Manucharyan et al. , Physical Review B, 76 014524 (2017)